Insulin signaling mediates neurodegeneration in glioma

Patricia Jarabo[1], Carmen de Pablo[1], Héctor Herranz[2], Francisco Antonio Martín[1*] and Sergio Casas-Tintó[1*]

1- Instituto Cajal, CSIC, Madrid, Spain.

2- University of Copenhagen, Copenhagen, Denmark.

*Equal contribution

Corresponding authors scasas@cajal.csic.es and famartin@cajal.csic.es

Key words: ImpL2, synapse, Insulin signaling, glia, neuron, cell to cell signaling, Drosophila, brain tumor, miR-8, microRNAs

Abstract

Cell to cell communication facilitates tissue development and physiology. Under pathological conditions, brain tumors disrupt glia-neuron communication signals in which in consequence, promotes tumor expansion at expenses of healthy tissue. The glioblastoma is the most aggressive and frequent brain tumor. This type of glioma expands and infiltrates in the brain, causing neuronal degeneration and neurological decay, among other symptoms. Here we describe how glioblastoma produce ImpL2, an antagonist of the insulin pathway, which is regulated by the microRNA miR-8. ImpL2 targets neighboring neurons and causes mitochondrial disruption as well as synapse loss, an early symptom of neurodegeneration. Furthermore, glioblastoma progression requires insulin pathway attenuation in neurons. Restoration of neuronal insulin activity is sufficient to rescue this synapse loss and delay the premature death caused by glioma. Therefore, signals from GB to neuron emerge as a potential field of study to prevent neurodegeneration and anti-tumoral strategies.

Introduction

Cancer is one of the leading causes of mortality worldwide and is expected to be responsible for 15 million deaths in 2020 (65% in less developed countries) according to the World Health Organization. Notwithstanding recent advances in health treatments and extended lifespan of patients, some tumors remain still incurable. Among them, glioblastoma (GB) stands out: this is the most frequent and aggressive primary brain tumor, originated from glial cells and causing death within the first year after diagnosis (Bi and Beroukhim, 2014). This is accompanied by broad neurological dysfunctions, despite standard treatments such as resection, radiotherapy, and chemotherapy (Messaoudi et al., 2015). Brain tumors cause cognitive decline and neuronal dysfunction (reviewed in (Bergo et al., 2016; Gehrke et al., 2013). These cognitive defects are consistent with typical neurodegenerative-associated symptoms (Granholm et al., 2008; Levenson et al., 2014).

Drosophila melanogaster, the fruit fly, has emerged as a reliable animal system to mimic human diseases such as cancer (Sonoshita and Cagan, 2017). However, the aim is not to heal a sick insect but to model cellular and molecular mechanisms of human diseases, in order to identify targets for eventual diagnosis and treatments of patients. The power of *Drosophila* genetics allows genetic and pharmacological screens that may be translated to medicine, particularly for neurodegenerative disorders (Burke et al., 2017; Casas-Tinto et al., 2011; Dar et al., 2012; Held et al., 2019; Metwally et al., 2019; Portela et al., 2019a). In fact, a *Drosophila* GB model that recapitulates most of the human disease features

has been developed and validated (Portela et al., 2019a; Read, 2011; Read et al., 2009; Read et al., 2013). This model is based on two of the most frequent mutations in patients, a constitutively active form of EGFR (dEGFRλ) and the PI3K catalytic subunit p110α (PI3K92E) driven by the glial specific *repo-Gal4* (Read et al., 2009). This animal model has brought novel understandings into glioblastoma molecular mechanisms (Chen and Read, 2019; Portela et al., 2019a; Portela et al., 2019b; Read et al., 2013).

MicroRNAs (miRNAs) are short non-coding RNAs that control gene activity mainly through post-transcriptional mechanisms. They m have been related recently to almost all biological processes and diseases, particularly cancer (Peng and Croce, 2016; Sander and Herranz, 2019). Related to glioma, the *miR-200* family (which includes *miR-200*, *miR-141* and *miR-429*) plays central roles in GB development, metastasis, therapeutic response, and prognosis (reviewed by (Peng et al., 2018)). Low levels of *miR-200* are indicative of poor prognosis in GB (Men et al., 2014). In colorectal cancer and GB, low expression levels of micro-RNAs correlates with up-regulation of *insulin-like growth binding protein 7* (*IGFBP7*) (Jones et al., 2015). Likewise, in GB there is a TGFB2-dependent increase in IGFBP7 protein levels (Pen et al., 2008). However, the mechanisms involved in IGFBP7 influence on GB progression and its regulation by *miR-200* remains unsolved. In *Drosophila*, *miR-200* and *IGFBP7* are represented by *miR-8* and *Imaginal morphogenesis protein-late 2* (*ImpL2*), respectively (Honegger et al., 2008). In juvenile stages, *miR-8* has been related to glial cell growth and regulates positively synaptic growth at the neuromuscular junction (Loya et al., 2014; Morante et al., 2013).

In contrast, *Drosophila ImpL2* is related to cachexia, a systemic effect characterized by anorexia and metabolic alterations in other malignant tumors (Petruzzelli and Wagner, 2016). Secreted ImpL2 from epithelial tumor cells induces systemic organ wasting and insulin resistance by antagonizing insulin signaling (Figueroa-Clarevega and Bilder, 2015; Kwon et al., 2015). Interestingly, PI3K and dRheb, two members of the insulin pathway, induce the formation of synapsis between neurons (a process known as synaptogenesis) in *Drosophila* larval brain (Martin-Pena et al., 2006). Actually, it has been shown that AKT, also involved in insulin signaling, acts as a pro-synaptogenic element (Jordan-Alvarez et al., 2017). These data strongly support a role for insulin signaling in the regulation of neuronal synaptic activity in *Drosophila*. In mammals, a similar effect of insulin signaling on synaptic plasticity has been described (Knafo and Esteban, 2017). Notably, synapse loss is an early step in neurodegeneration (Henstridge et al., 2016; Sephton and Yu, 2015). We have recently re-evaluated GB as a neurodegenerative disease, showing that GB reduces the number of synapsis through wingless/frizzled 1 (wg/fz1) signaling (Portela et al, PLOS Biol 2019), equivalent to mammalian wnt pathway (Arnes and Casas Tinto, 2017). However, whether tumoral glial cells are able to modify insulin signaling directly in neurons, and consequently alter the number of synapses, is not known yet.

In this report, we show that secreted ImpL2 from glial-derived tumoral cells antagonizes insulin signaling in neighboring neurons, inducing a reduction in synapse number and consequently promoting neurodegeneration. *ImpL2* expression in GB cells is regulated by *miR-8*, thus linking functionally micro-RNA pathway with Insulin signaling in a GB model. We describe the function of ImpL2 as a mediator in GB-neuron communication, responsible for the reduction in

synapse number and neurological defects. Indeed, we propose the insulin pathway as a core signal in GB progression and neurological decay. Finally, we propose a novel neuroprotective strategy against GB that extend lifespan and improve life quality.

Results

ImpL2 mediates GB progression and neurodegeneration

To study the mechanisms of communication among malignant glial cells and neurons, we used a previously described *Drosophila* GB model that stimulates the oncogenic transformation of glial cells in post-embryonic larval (Read et al., 2009; Read et al., 2013) or adult brains (Portela et al., 2019a), leading to lethal glial neoplasia. We previously reported a reduction in the number of synapses in the neuromuscular junction (NMJ) of adult flies caused by GB progression (Portela et al, 2019). This neurodegenerative process is observed even though those genetic modifications were caused in glial cells. This phenomenon suggests that signals originated in the glial tumor impact on neighboring neurons. Synaptogenesis is tightly regulated by PI3K, a main player in insulin signaling pathway (Jordan-Alvarez et al., 2017). Moreover, the expression of secreted molecules that decrease insulin pathway activity, such as ImpL2 (IGFBP7 in humans), correlates with GB progression (Jones et al., 2015; Pen et al., 2008).

To determine *ImpL2* mRNA expression levels in GB we performed qPCR experiments. *ImpL2* mRNA shows an increase in GB samples as compared to control brains (fig 1A). To discriminate *ImpL2* expression in neuronal or glial (GB)

cells, we used a MIMIC GFP reporter that reproduces faithfully ImpL2 expression (Nagarkar-Jaiswal et al., 2015). Consistently, GB cells show higher GFP levels than control glial cells. Likewise, upon *ImpL2* RNAi expression we detect a decrease in GFP levels, similar to the ones observed in control brains (fig 1B-D). In a previous work we established that tumoral progression depends on the formation of a network of protrusions (i.e. an expansion of the membrane surface) named tumor microtubules (TMs), similarly to human glioblastoma (Osswald et al., 2015; Portela et al., 2019b). Besides, in mammals and flies the TM network requires the *GAP43* and *igloo* gene functions, respectively (Osswald et al., 2015; Portela et al., 2019b). We also showed that GB progression requires c-Jun N-terminal Kinase (JNK) pathway activity (Portela et al., 2019b). The *Drosophila* JNK homolog *basket* (*bsk*) plays a central role in JNK signaling in normal and tumoral conditions (Fahey-Lozano et al., 2019). We overexpressed *igloo RNAi* and a dominant negative form of *bsk* to block TM formation and JNK activity, respectively. As expected, ImpL2 expression levels are reverted to similar levels to the ones observed in controls brains in both cases (fig 1E-F). Indeed, using an analysis of co-localization rate between ImpL2 and glial cells we see a significant increase in ImpL2 levels specifically in GB cells (fig 1G).

To detect signs of neurodegeneration, we quantify the number of synapses in the neuromuscular junction (NMJ) of the adult flies with GB. NMJ is a stereotyped structure to count the number of active zones (AZ) in the synaptic buttons of the motoneurons (see material and methods for details). To determine the contribution of *ImpL2* in synapse loss, we knockdown *ImpL2* in GB cells and counted the number of active zones in adult NMJs. The results show that *ImpL2* reduction in GB cells counteracted the reduction in the number of active zones of

GB brains (fig 2A-C, E). Consistently, *ImpL2* over-expression in wild type (wt) glial cells decreases the number of AZ in NMJs (fig 2D-E). Two additional and typical features of GB are the increase in the number of glial cells and the expansion of a TM network (Portela et al., 2019b) (Fig 2F-G, I-J). As expected, the down-regulation of Impl2 RNA levels in GB causes a striking reduction in the number of glial cells (fig 2H-I) and in the total tumor volume (2J).

Thus, we conclude that GB cells upregulate and secrete ImpL2, a necessary step to induce tumoral expansion and a reduction of AZ number.

microRNAs regulate *ImpL2* expression in GB

It has been described that low levels of micro-RNAs correlate with high levels of ImpL2 homolog in human GB, suggesting that Impl2 regulation might be mediated by microRNAs (Jones et al., 2015). Accordingly, there is a down-regulation of the microRNA *miR-200* family in GB samples (reviewed in (Peng et al., 2018)) Given that *miR-8*, the Drosophila homologue of *miR-200* family, regulates negatively ImpL2 mRNA stability in the fat body (Lee et al., 2015)), we hypothesize that *miR-8* might play a role in GB progression regulating Impl2 levels. We used a *miR-8* sensor to monitor *miR-8* activity. It includes *miR-8* binding sites in the 3´UTR of the *GFP* gene (Kennell et al., 2012). Thus, high levels of GFP indicates low levels of *miR-8* activity, and vice versa (see Materials and Methods). GFP signal is increased in GB cells (fig 3A-C), indicating that *miR-8* levels are reduced. To determine if the increase of *ImpL2* in GB depend on *miR-8*, we analyzed *ImpL2* sensor upon *miR-8* overexpression in that context. We observed a significant reduction of *ImpL2* expression in GB cells *in vivo*. Consistently, *miR-8* gain-of-function in GB partially rescues the loss of synapses,

recapitulating *ImpL2* loss-of-function in GB conditions (fig 3D-G). In addition, the reduction of AZs number in NMJ caused by the GB can be attenuated by *miR-8* overexpression in GB cells (fig 3H-J, L), compatible with the effect of *ImpL2* down-regulation (fig 2C). Furthermore, *miR-8* overexpression in wt glial cells (with low *ImpL2* levels) does not alter the number of AZ (fig 3K-L). Intriguingly, GB cell number expansion is not prevented by *miR-8* overexpression (fig 3M-O, Q), and consistently *miR-8* overexpression does not change glial cell number in wt conditions (fig 3P-Q). However, we do observe a reduction of GB membrane volume upon *miR-8* upregulation, something that does not occur in normal glial cells (fig 3R). Altogether these results show an inverse correlation between miR-8 and Impl2 expression in GB cells and suggest that ImpL2 levels are regulated by *miR-8 in vivo*.

GB secreted ImpL2 reduces neuronal Insulin signaling

To evaluate the impact of Insulin signaling reduction in neurons, we measure *dRheb* mRNA by qPCR. d*Rheb* is the molecular link between insulin signaling pathway and TOR kinase, and it reflects the Insulin pathway activity (reviewed in (Armijo et al., 2016)): d*Rheb mRNA* levels drop down when Insulin signaling is low (Garami et al., 2003). We analyzed d*Rheb* expression levels in control and GB brains. The GB itself is induced by overexpressing a constitutively active form of PI3K, thusactivated insulin pathway in all glial cells. However, the majority of brain cells are neurons (up to 90%) (Freeman, 2015), so we reasoned that a qPCR would reflect mostly neuronal expression. Accordingly, mRNA levels of *dRheb* are reduced in GB brains when compared with control brains (fig 4E).

To further analyze insulin-dependent TOR activity we used a *THOR-MIMIC* line. In normal conditions, *thor* transcription remains at low but detectable levels (Teleman et al., 2005). However, when Insulin activity is compromised, *thor* is highly transcribed, as reflected by *LacZ*- or *MIMIC- THOR* lines (Galagovsky et al., 2014). Neurons confronted with GB cells have reduced Insulin signaling, as shown by *THOR-MIMIC* GFP expression. This effect on Insulin pathway is restored by down-regulating *ImpL2* in GB cells (fig 4A-D). All these results together suggest that *ImpL2* up-regulation in GB cells mediates the decreased insulin pathway activity detected in neurons.

However, the central function for insulin signaling pathway related to synaptogenesis was described mainly in larval NMJ synapsis (Martin-Pena et al., 2006). Whether or not insulin signaling plays a similar role in the central adult nervous system has not been evaluated yet. To do so, we expressed a dominant negative form of the *insulin receptor (InR)* in motor neurons. We stained with anti-bruchpilot and quantified the number of active zones. This number was reduced when compared with control (fig 4 F-I). Moreover, high levels of secreted ImpL2 from glial cells shows also a reduction in the synapse number, thus suggesting that the ImpL2 effect on synapsis is due to a regulation of Insulin signaling.

Insulin signaling in neurons mediates neurodegeneration and mortality in GB.

To determine if the restoration of Insulin pathway activity prevents neurodegeneration in GB samples we upregulated *Rheb* in neurons. However, in order to manipulate Insulin pathway activity in neuronal population simultaneously with GB induction in glial cells, we needed to use the

LexA/LexAOp system (see Materials and Methods). We overexpressed *LexAOp-*d*Rheb* (thus activating Insulin signaling) in neurons using an *elav-LexA* line. d*Rheb mRNA* levels increase significantly upon LexA/LexAop system activation, therefore validating the *LexAop-Rheb* tool (fig 4E). The quantifications of adult NMJs show an increase in the number of AZ in NMJ when compared to GB and even to control genotypes, thus showing a similar effect (although slightly stronger) to GB with low ImpL2 levels (fig 5A-C, G). In conclusion, the larval synaptogenic pathway regulated by Insulin pathway members seems to be conserved in adult brains, at least for *InR* and *dRheb*.

Insulin signaling mediates glucose metabolism and mitochondrial physiology (Cheng et al., 2010). Additionally, mitochondrial alterations are related with synapse dysfunction and neurodegeneration (Zhao et al., 2019) (Chen et al., 2019). Therefore, we investigated if GB progression affects neuronal mitochondria. In particular, the transport of mitochondria through the axons is altered in other neurodegenerative diseases (Vanhauwaert et al., 2019).

We used a *lexAop-mitocherry* reporter transgene to quantify the distribution of mitochondria in axon terminals. Pixel intensity quantification showed that GB causes a significant increase of mitochondria in the neuronal projections of Kenyon cells in the mushroom body (fig 5 D-F, D'-F', H), compatible with a neurodegenerative process (Chevalier-Larsen and Holzbaur, 2006). In line with this, we observed an increase of mitochondria accumulated in the buttons of the NMJs that correlates with lower number of synaptic buttons (5D''-F'', I). Both effects in neuronal projections and NMJs are prevented upon Insulin pathway signaling activation in the neuronal population of a GB brain (fig 5F, F', F''). Consistently, electron microscopy images of neuronal mitochondria in GB

samples show defects in the cristae, a typical feature of non-functional mitochondria (Long et al., 2015; Miyazono et al., 2018). This mitochondrial defective morphology is also reverted upon d*Rheb* overexpression in neurons (fig 5 J-L). Altogether, these results indicate that despite the higher number of mitochondria, neurons show dysfunctional mitochondria as a consequence of low insulin signaling. Increasing insulin pathway activity in neurons exposed to GB may be sufficient to recover functional organelles, as suggested by the synapse number.

GB brains with high insulin signaling in neurons also show a reduction in the number of glial cells and in the GB volume (fig 6 A-E). More importantly, GB causes premature death, an effect that is significantly rescued by overexpressing d*Rheb* in neurons (fig 6 F). These results suggest that restoration of neuronal insulin pathway activity improves the lifespan in animals with GB, thus linking synaptogenesis to a slower disease progression and providing a possible novel therapeutic target.

DISCUSSION

Glioblastoma is the most aggressive type of brain tumor. During GB progression tumoral cells emit projections known as tumor microtubes that contribute to brain infiltration and to a poor prognosis for the patient. GB courses with a neurological decay that includes drowsiness, sleep disturbances, speech difficulties and other typical symptoms of neurodegeneration (Bergo et al., 2016). For decades the origin of this decay was attributed to the high pressure caused by the GB solid mass and the associated edema. Despite the solid mass of GB is removed after surgery, the neurodegenerative process continues, more likely due to the diffuse

GB progression. This indicates that mechanisms underlying neurological decay are not restricted to the intracranial pressure and edema.

Recent publications suggested an active communication between GB cells and the surrounding healthy tissue, including neurons. Experiments done with human GB cells in mice xenografts revealed a physical interaction between GB cells and neurons as electrical and chemical synapses (Venkataramani et al., 2019; Venkatesh et al., 2019). In this case neurons act as presynaptic structures whereas GB tumoral cells are postsynaptic elements. These so-called "synapses" are required for GB progression. Besides, we have recently described cellular mechanisms for GB to deplete Wingless (Wg)/WNT from neurons. GB cells project TMs that enwrap neurons and accumulate Frizzled1 (Fz1) receptor to vampirize Wg from neighboring neurons. This unidirectional mechanism facilitates GB proliferation and cause a loss of synapses in the neurons (Portela et al., 2019b). Finally, here we also describe a one-way communication system from GB cells towards neurons. ImpL2 protein is originated in GB cells and target healthy neurons, but not vice-versa. ImpL2 binds InR ligands and act as an antagonist of the pathway. In consequence, InR signaling is lowered in neurons which in turn cause mitochondrial aberrations, synapse loss and functional decline. Neuronal insulin signaling can be restored via *Rheb* upregulation, and this is sufficient to extend the lifespan of GB animals. These results suggest that lowering insulin signaling (and the subsequent neurodegeneration) is critical for the lethality caused by GB.

The regulation of *ImpL2* expression in GB cells seems to depend on microRNAs, at least in part. In cancer, micro-RNAs have emerged as general regulators key for tumoral progression, including GB (Sander and Herranz, 2019). Interestingly,

miR-200 family (*miR-8* in *Drosophila*) play a key role in human GB. We have described the presence and relevance of *miR-8* in GB progression as a regulator of *ImpL2* expression. However, there are no predicted *miR-8* binding sites in *ImpL2* sequence; therefore, it is unlikely that *miR-8* regulates directly *ImpL2 mRNA* stability. One possibility is the existence of mediator proteins that depend directly on *miR-8*. The most evident possibility is a transcription factor whose mRNA stability is sensitive to *miR-8* and acts as a transcriptional regulator of *ImpL2.* However, the regulation of *ImpL2* and the relation with microRNAs is a matter of future studies. Another intriguing point is the different effects on GB growth that have *miR-8* overexpression and *Impl2* down-regulation. Whereas an excess of *miR-8* is unable to reduce GB cell number, lacking *Impl-2* reduces significantly the growth of GB cells. However, it is known that most of microRNAs control several mRNAs, thus *miR-8* overexpression might affect to different extent other *mRNAs* than just *ImpL2* mRNA, which can account for such differences.

Taking all these conclusions together, is tempting to affirm that the progression of brain tumors in *Drosophila* depends not only in the intrinsic properties of the tumoral cells, but also in the physiological condition of the surrounding cells. GB patients respond differently to the progression of the GB: some patients survive for a few months whereas others survive for years. If we accept that the coordinated effect in GB and neurons result in differential tumor progression, the vast differences in how patients respond to GB could be, in part, dependent on genetic or epigenetic conditions related to InR signaling genes in neurons, and probably other pathways such as WNT or Hedgehog.

Materials and methods

Fly stocks and genetics

All fly stocks were maintained at 25ºC (unless otherwise specified) on a 12/12h light/dark cycles at constant humidity in standard medium. The stocks used from Bloomington Stock Center were: *tub-Gal80^{ts}* (BL-7019), *Repo-Gal4* (BL-7415*), D42-Gal4* (BL-8816), *UAS-InR DN* (Bl-2852), *UAS-myr-RFP* (BL-7119) *UAS-LacZ* (BL-8529), *UAS-ImpL2RNAi* (BL-55855), *UAS-ImpL2MIMIC* (BL-59246), *lexAop-mitocherry* (BL-66530). Others fly stocks used were: *UAS-miR-8-sensor* (Kennell et al., 2012), *UAS-miR-8-RFP* (Lu et al., 2014), *Elav-LexA* (BL52676), *lexAop-Rheb*, *UAS-HRP::CD2 (*gifted by L.Luo, Watts el al., 2004), *UAS-dEGFR$^{\lambda}$*;*UAS-dp110^{CAAX}* (gift from R. Read, Read et al., 2009) *UAS-ImpL2* (gift from H. Stocker), LexAop-Rheb, (gift from Nuria Romero).

The glioma-inducing line contains the *UAS-dEGFR$^{\lambda}$*, *UAS-dp110^{CAAX}* transgenes that encodes for the constitutively active forms of the human orthologues PI3K and EGFR respectively (Read et al., 2009). *Repo-Gal4* line drives the *Gal4* expression in every glial cell (Lee and Jones, 2005) and combined with the *UAS-dEGFR$^{\lambda}$*, *UAS-dp110^{CAAX}* line allow us to generate a glioma thanks to the Gal4 system (Brand and Perrimon, 1993). *Elav-LexA* line drives the expression to neurons (Campos et al., 1987), permiting us to manipulate neurons in a glioma combining *LexA* and *Gal4* expression systems (Lai and Lee, 2006).

Gal80^{TS} is able to inhibit the Gal4 activity at 18ºC, though at 29ºC is inactivated (McGuire et al., 2003). The *tub-Gal80^{ts}* construct was used in all the crosses to avoid the lethality during the larval stage cause by the glioma development. Until the adult flies emerged, the crosses were kept at 17ºC. To inactivate the Gal80^{ts} protein and activate the *Gal4* expression of our genes of interest, the adult flies were maintained at 29ºC as many days as indicate in each experiment.

Immunostaining and Image acquisition

Adult brains were dissected and fixed with 4% formaldehyde in phosphate-buffered saline for 20 minutes whereas adult NMJ were fixed 10 minutes; in both cases, samples were washed 3x15 min with PBS+0.4% triton, blocked for 1 h with BSA 1%, incubated overnight with primary antibodies, washed 3x15 min, incubated with secondary antibodies for 4 h and mounted in Vectashield mounting medium with DAPI. The primary antibodies used were anti-repo mouse (1/200, DSHB), anti-nc82

mouse (1/50, DSHB), anti-HRP rabbit (1/400, Cell Signalling) anti-GFP rabbit (1:500, DSHB). The secondary antibodies used were Alexa 488 or 647 (1/500, Life Technologies). Images were taken by a Leica SP5 confocal microscopy. To quantify active zones and number of glial cells, we analyzed confocal images with the Imaris software (www.bitplane.com). It allows to select intensity points of a specific diameter that correspond either to the active zones (0.5 µm) or glial cell nuclei (2 µm). Using this software, it is also possible to determine the volume of the glial membrane. For the analysis of pixel intensity, the "measurement log" tool of Photoshop CS5 was used. For the analysis of co-localization rates, "co-localization" tool from LAS AF Lite software (Leica) was used.

RNA extraction, reverse transcription and qPCR

For RNA extraction, 1- to 4- day-old male adults were entrained to a 12:12 h LD cycle for 7 days at 29ºC and then collected on dry ice at ZT 6. Total RNA was extracted from 30 heads of adult males of the Control (*repo>LacZ*), Glioma (*repo> UAS-dEGFR*$^{\lambda}$, *UAS-dp110*^{CAAX}) and *repo> UAS-dEGFR*$^{\lambda}$, *UAS-dp110*^{CAAX}*, elav-LexA, LexAOp-Rheb* genotypes after 7 days of glioma development. RNA was extracted with TRIzol and phenol chloroform. Total RNA concentration was measured by using NanoDrop ND-1000. cDNA was synthetized from 1 mg of total RNA using M-MLV RT (Invitrogen). cDNA samples from 1:5 dilutions were used for real-time PCR reactions. Transcription levels were determined in a 14 mL volume in duplicate using SYBR Green (Applied Biosystem, Foster City, CA) and 7500qPCR (Thermo Fisher, Waltham, MA). We analysed transcription levels of *ImpL2*, *Rheb* and *Rp49* as housekeeping gene reference.

Sequences of primers were: RP49 F: GCATACAGGCCCAAGATCGT, Rp49 R: AACCGATGTTGGGCATCAGA, ImpL2 F: CCGAGATCACCTGGTTGAAT, ImpL2 R: AGGTATCGGCGGTATCCTTT, Rheb F: CGACGTAATGGGCAAGAAAT and Rheb R: CAAGACAACCGCTCTTCTCC.

After completing each real-time PCR run, outlier data were analysed using 7500 software (Applied Biosystems). Ct values of triplicates from 3 biological samples were analysed calculating 2DDCt and comparing the results using a t-test with GraphPad (GraphPad Software, La Jolla, CA).

Viability and survival assays.

Lifespan was determined under 12:12 h LD cycles at 29ºC conditions. Three replicates of 30 1- to 4- day-old male adults were collected in vials containing standard *Drosophila* media and transferred every 2-3 days to fresh *Drosophila* media.

Electron microscopy

Adult brains of *repo>LacZ, repo> UAS-dEGFR*$^{\lambda}$, *UAS-dp110*^{CAAX} and *repo> UAS-dEGFR*$^{\lambda}$, *UAS-dp110*^{CAAX}*, elav-LexA, LexAOp-Rheb* animals expressing CD2-HRP in glial membranes were dissected after 7 days of glioma development and fixed with 4% formaldehyde in phosphate-buffered saline for 30 minutes. The samples were washed twice with PBS and incubate with R.T.U. VECTASTAIN kit (VECTOR) for 30 min at RT and washed once with PBS. Followed by an incubation in darkens with SIGMA FAST 3,3'- Diaminobenzidine Tablet SETS (SIGMA) for 75 min at RT, washed once with PBT and incubate with 4% formaldehyde + 2% glutaraldehyde for 1 hour and store at 4ºC. Following fixation samples were washed three times in 0.1 m phosphate buffer. Postfixation was done in 1% osmium tetroxide + 1% potassium ferrocyanide for 1 hour at 4ºC, three washes in H2O2dd and incubated in PBS 0.1M + 0.15% tanic acid for 1 min, washed once in PBS 0.1M and twice in H2O2dd. Following by incubation in 2% uranil acetate 1 hour at RT in darkness and three washes in H2O2dd. Dehydration was done in ethanol series (30%, 50%, 70%, 90% and 3x100%). The samples were infiltrated with increasing concentrations of epoxy resin TAAB-812 (TAAB Laboratories) in propilen oxid, encapsulated in BEEM capsules to polymerize 48 hours at 60ºC. Ultrathin sections of 70-80 nm were cut using Ultracut E microtome (Leica) and stained with 2% uranyl acetate solution in water and lead Reynols citrate. The grids were examined with JeolJEM1400Flash (Tokyo, Japan) electron microscope at 80 kV. Images were taken with a OneView (4Kx4K) CMOS camera (Gatan).

Statistics

The results were analyzed using the GraphPad Prism 5 software (www.graphpad.com). Quantitative parameters were divided into parametric and non parametic using the D'Agostino and Pearson omnibus normality test and the variances were analyzed with F test. Student' t test and ANOVA test with Bonferroni's post-hoc were used in parametric parameters, using Welch's correction when necessary. To the non-parametric parameters, Mann-Whitney test and Kruskal-

Wallis test with Dunns post-hoc were used. The survival assays were analyzed with Mantel-Cox test. The *p* limit value for rejecting the null hypothesis and considering the differences between cases as statistically significant was $p < 0.05$ (*). Others *p* values are indicated as ** when $p < 0.01$ and *** when $p < 0.001$.

References

Armijo, M. E., Campos, T., Fuentes-Villalobos, F., Palma, M. E., Pincheira, R. and Castro, A. F. (2016). Rheb signaling and tumorigenesis: mTORC1 and new horizons. *Int J Cancer* **138**, 1815-1823.

Arnes, M. and Casas Tinto, S. (2017). Aberrant Wnt signaling: a special focus in CNS diseases. *J Neurogenet* **31**, 216-222.

Bergo, E., Lombardi, G., Pambuku, A., Della Puppa, A., Bellu, L., D'Avella, D. and Zagonel, V. (2016). Cognitive Rehabilitation in Patients with Gliomas and Other Brain Tumors: State of the Art. *Biomed Res Int* **2016**, 3041824.

Bi, W. L. and Beroukhim, R. (2014). Beating the odds: extreme long-term survival with glioblastoma. *Neuro Oncol* **16**, 1159-1160.

Brand, A. H. and Perrimon, N. (1993). Targeted gene expression as a means of altering cell fates and generating dominant phenotypes. *Development* **118**, 401-415.

Burke, C., Trinh, K., Nadar, V. and Sanyal, S. (2017). AxGxE: Using Flies to Interrogate the Complex Etiology of Neurodegenerative Disease. *Curr Top Dev Biol* **121**, 225-251.

Campos, A. R., Rosen, D. R., Robinow, S. N. and White, K. (1987). Molecular analysis of the locus elav in Drosophila melanogaster: a gene whose embryonic expression is neural specific. *EMBO J* **6**, 425-431.

Casas-Tinto, S., Zhang, Y., Sanchez-Garcia, J., Gomez-Velazquez, M., Rincon-Limas, D. E. and Fernandez-Funez, P. (2011). The ER stress factor XBP1s prevents amyloid-beta neurotoxicity. *Hum Mol Genet* **20**, 2144-2160.

Chen, A. S. and Read, R. D. (2019). Drosophila melanogaster as a Model System for Human Glioblastomas. *Adv Exp Med Biol* **1167**, 207-224.

Chen, C., Turnbull, D. M. and Reeve, A. K. (2019). Mitochondrial Dysfunction in Parkinson's Disease-Cause or Consequence? *Biology (Basel)* **8**.

Cheng, Z., Tseng, Y. and White, M. F. (2010). Insulin signaling meets mitochondria in metabolism. *Trends Endocrinol Metab* **21**, 589-598.

Chevalier-Larsen, E. and Holzbaur, E. L. (2006). Axonal transport and neurodegenerative disease. *Biochim Biophys Acta* **1762**, 1094-1108.

Dar, A. C., Das, T. K., Shokat, K. M. and Cagan, R. L. (2012). Chemical genetic discovery of targets and anti-targets for cancer polypharmacology. *Nature* **486**, 80-84.

Fahey-Lozano, N., La Marca, J. E., Portela, M. and Richardson, H. E. (2019). Drosophila Models of Cell Polarity and Cell Competition in Tumourigenesis. *Adv Exp Med Biol* **1167**, 37-64.

Figueroa-Clarevega, A. and Bilder, D. (2015). Malignant Drosophila tumors interrupt insulin signaling to induce cachexia-like wasting. *Dev Cell* **33**, 47-55.

Freeman, M. R. (2015). Drosophila Central Nervous System Glia. *Cold Spring Harb Perspect Biol* **7**.

Galagovsky, D., Katz, M. J., Acevedo, J. M., Sorianello, E., Glavic, A. and Wappner, P. (2014). The Drosophila insulin-degrading enzyme restricts growth by modulating the PI3K pathway in a cell-autonomous manner. *Mol Biol Cell* **25**, 916-924.

Garami, A., Zwartkruis, F. J., Nobukuni, T., Joaquin, M., Roccio, M., Stocker, H., Kozma, S. C., Hafen, E., Bos, J. L. and Thomas, G. (2003). Insulin activation of Rheb, a mediator of mTOR/S6K/4E-BP signaling, is inhibited by TSC1 and 2. *Mol Cell* **11**, 1457-1466.

Gehrke, A. K., Baisley, M. C., Sonck, A. L., Wronski, S. L. and Feuerstein, M. (2013). Neurocognitive deficits following primary brain tumor treatment: systematic review of a decade of comparative studies. *J Neurooncol* **115**, 135-142.

Granholm, A. C., Boger, H. and Emborg, M. E. (2008). Mood, memory and movement: an age-related neurodegenerative complex? *Curr Aging Sci* **1**, 133-139.

Held, A., Major, P., Sahin, A., Reenan, R. A., Lipscombe, D. and Wharton, K. A. (2019). Circuit Dysfunction in SOD1-ALS Model First Detected in Sensory Feedback Prior to Motor Neuron Degeneration Is Alleviated by BMP Signaling. *J Neurosci* **39**, 2347-2364.

Henstridge, C. M., Pickett, E. and Spires-Jones, T. L. (2016). Synaptic pathology: A shared mechanism in neurological disease. *Ageing Res Rev* **28**, 72-84.

Honegger, B., Galic, M., Kohler, K., Wittwer, F., Brogiolo, W., Hafen, E. and Stocker, H. (2008). Imp-L2, a putative homolog of vertebrate IGF-binding protein 7, counteracts insulin signaling in Drosophila and is essential for starvation resistance. *J Biol* **7**, 10.

Jones, T. A., Jeyapalan, J. N., Forshew, T., Tatevossian, R. G., Lawson, A. R., Patel, S. N., Doctor, G. T., Mumin, M. A., Picker, S. R., Phipps, K. P., et al. (2015). Molecular analysis of pediatric brain tumors identifies microRNAs in pilocytic astrocytomas that target the MAPK and NF-kappaB pathways. *Acta Neuropathol Commun* **3**, 86.

Jordan-Alvarez, S., Santana, E., Casas-Tinto, S., Acebes, A. and Ferrus, A. (2017). The equilibrium between antagonistic signaling pathways determines the number of synapses in Drosophila. *PLoS One* **12**, e0184238.

Kennell, J. A., Cadigan, K. M., Shakhmantsir, I. and Waldron, E. J. (2012). The microRNA miR-8 is a positive regulator of pigmentation and eclosion in Drosophila. *Dev Dyn* **241**, 161-168.

Knafo, S. and Esteban, J. A. (2017). PTEN: Local and Global Modulation of Neuronal Function in Health and Disease. *Trends Neurosci* **40**, 83-91.

Kwon, Y., Song, W., Droujinine, I. A., Hu, Y., Asara, J. M. and Perrimon, N. (2015). Systemic organ wasting induced by localized expression of the secreted insulin/IGF antagonist ImpL2. *Dev Cell* **33**, 36-46.

Lai, S. L. and Lee, T. (2006). Genetic mosaic with dual binary transcriptional systems in Drosophila. *Nat Neurosci* **9**, 703-709.

Lee, B. P. and Jones, B. W. (2005). Transcriptional regulation of the Drosophila glial gene repo. *Mech Dev* **122**, 849-862.

Lee, G. J., Jun, J. W. and Hyun, S. (2015). MicroRNA miR-8 regulates multiple growth factor hormones produced from Drosophila fat cells. *Insect Mol Biol* **24**, 311-318.

Levenson, R. W., Sturm, V. E. and Haase, C. M. (2014). Emotional and behavioral symptoms in neurodegenerative disease: a model for studying the neural bases of psychopathology. *Annu Rev Clin Psychol* **10**, 581-606.

Long, Q., Zhao, D., Fan, W., Yang, L., Zhou, Y., Qi, J., Wang, X. and Liu, X. (2015). Modeling of Mitochondrial Donut Formation. *Biophys J* **109**, 892-899.

Loya, C. M., McNeill, E. M., Bao, H., Zhang, B. and Van Vactor, D. (2014). miR-8 controls synapse structure by repression of the actin regulator enabled. *Development* **141**, 1864-1874.

Lu, C. S., Zhai, B., Mauss, A., Landgraf, M., Gygi, S. and Van Vactor, D. (2014). MicroRNA-8 promotes robust motor axon targeting by coordinate regulation of cell adhesion molecules during synapse development. *Philos Trans R Soc Lond B Biol Sci* **369**.

Martin-Pena, A., Acebes, A., Rodriguez, J. R., Sorribes, A., de Polavieja, G. G., Fernandez-Funez, P. and Ferrus, A. (2006). Age-independent synaptogenesis by phosphoinositide 3 kinase. *J Neurosci* **26**, 10199-10208.

McGuire, S. E., Le, P. T., Osborn, A. J., Matsumoto, K. and Davis, R. L. (2003). Spatiotemporal rescue of memory dysfunction in Drosophila. *Science* **302**, 1765-1768.

Men, D., Liang, Y. and Chen, L. (2014). Decreased expression of microRNA-200b is an independent unfavorable prognostic factor for glioma patients. *Cancer Epidemiol* **38**, 152-156.

Messaoudi, K., Clavreul, A. and Lagarce, F. (2015). Toward an effective strategy in glioblastoma treatment. Part I: resistance mechanisms and strategies to overcome resistance of glioblastoma to temozolomide. *Drug Discov Today* **20**, 899-905.

Metwally, E., Zhao, G., Li, W., Wang, Q. and Zhang, Y. Q. (2019). Calcium-Activated Calpain Specifically Cleaves Glutamate Receptor IIA But Not IIB at the Drosophila Neuromuscular Junction. *J Neurosci* **39**, 2776-2791.

Miyazono, Y., Hirashima, S., Ishihara, N., Kusukawa, J., Nakamura, K. I. and Ohta, K. (2018). Uncoupled mitochondria quickly shorten along their long axis to form indented spheroids, instead of rings, in a fission-independent manner. *Sci Rep* **8**, 350.

Morante, J., Vallejo, D. M., Desplan, C. and Dominguez, M. (2013). Conserved miR-8/miR-200 defines a glial niche that controls neuroepithelial expansion and neuroblast transition. *Dev Cell* **27**, 174-187.

Nagarkar-Jaiswal, S., Lee, P. T., Campbell, M. E., Chen, K., Anguiano-Zarate, S., Gutierrez, M. C., Busby, T., Lin, W. W., He, Y., Schulze, K. L., et al. (2015). A library of MiMICs allows tagging of genes and reversible, spatial and temporal knockdown of proteins in Drosophila. *Elife* **4**.

Osswald, M., Jung, E., Sahm, F., Solecki, G., Venkataramani, V., Blaes, J., Weil, S., Horstmann, H., Wiestler, B., Syed, M., et al. (2015). Brain tumour cells interconnect to a functional and resistant network. *Nature* **528**, 93-98.

Pen, A., Moreno, M. J., Durocher, Y., Deb-Rinker, P. and Stanimirovic, D. B. (2008). Glioblastoma-secreted factors induce IGFBP7 and angiogenesis by modulating Smad-2-dependent TGF-beta signaling. *Oncogene* **27**, 6834-6844.

Peng, L., Fu, J. and Ming, Y. (2018). The miR-200 family: multiple effects on gliomas. *Cancer Manag Res* **10**, 1987-1992.

Peng, Y. and Croce, C. M. (2016). The role of MicroRNAs in human cancer. *Signal Transduct Target Ther* **1**, 15004.

Petruzzelli, M. and Wagner, E. F. (2016). Mechanisms of metabolic dysfunction in cancer-associated cachexia. *Genes Dev* **30**, 489-501.

Portela, M., Segura-Collar, B., Argudo, I., Saiz, A., Gargini, R., Sanchez-Gomez, P. and Casas-Tinto, S. (2019a). Oncogenic dependence of glioma cells on kish/TMEM167A regulation of vesicular trafficking. *Glia* **67**, 404-417.

Portela, M., Venkataramani, V., Fahey-Lozano, N., Seco, E., Losada-Perez, M., Winkler, F. and Casas-Tinto, S. (2019b). Glioblastoma cells vampirize WNT from neurons and trigger a JNK/MMP signaling loop that enhances glioblastoma progression and neurodegeneration. *PLoS Biol* **17**, e3000545.

Read, R. D. (2011). Drosophila melanogaster as a model system for human brain cancers. *Glia* **59**, 1364-1376.

Read, R. D., Cavenee, W. K., Furnari, F. B. and Thomas, J. B. (2009). A drosophila model for EGFR-Ras and PI3K-dependent human glioma. *PLoS Genet* **5**, e1000374.

Read, R. D., Fenton, T. R., Gomez, G. G., Wykosky, J., Vandenberg, S. R., Babic, I., Iwanami, A., Yang, H., Cavenee, W. K., Mischel, P. S., et al. (2013). A kinome-wide RNAi screen in Drosophila Glia reveals that the RIO kinases mediate cell proliferation and survival through TORC2-Akt signaling in glioblastoma. *PLoS Genet* **9**, e1003253.

Sander, M. and Herranz, H. (2019). MicroRNAs in Drosophila Cancer Models. *Adv Exp Med Biol* **1167**, 157-173.

Sephton, C. F. and Yu, G. (2015). The function of RNA-binding proteins at the synapse: implications for neurodegeneration. *Cell Mol Life Sci* **72**, 3621-3635.

Sonoshita, M. and Cagan, R. L. (2017). Modeling Human Cancers in Drosophila. *Curr Top Dev Biol* **121**, 287-309.

Teleman, A. A., Chen, Y. W. and Cohen, S. M. (2005). Drosophila Melted modulates FOXO and TOR activity. *Dev Cell* **9**, 271-281.

Vanhauwaert, R., Bharat, V. and Wang, X. (2019). Surveillance and transportation of mitochondria in neurons. *Curr Opin Neurobiol* **57**, 87-93.

Venkataramani, V., Tanev, D. I., Strahle, C., Studier-Fischer, A., Fankhauser, L., Kessler, T., Korber, C., Kardorff, M., Ratliff, M., Xie, R., et al. (2019). Glutamatergic synaptic input to glioma cells drives brain tumour progression. *Nature* **573**, 532-538.

Venkatesh, H. S., Morishita, W., Geraghty, A. C., Silverbush, D., Gillespie, S. M., Arzt, M., Tam, L. T., Espenel, C., Ponnuswami, A., Ni, L., et al. (2019). Electrical and synaptic integration of glioma into neural circuits. *Nature* **573**, 539-545.

Zhao, X. Y., Lu, M. H., Yuan, D. J., Xu, D. E., Yao, P. P., Ji, W. L., Chen, H., Liu, W. L., Yan, C. X., Xia, Y. Y., et al. (2019). Mitochondrial Dysfunction in Neural Injury. *Front Neurosci* **13**, 30.

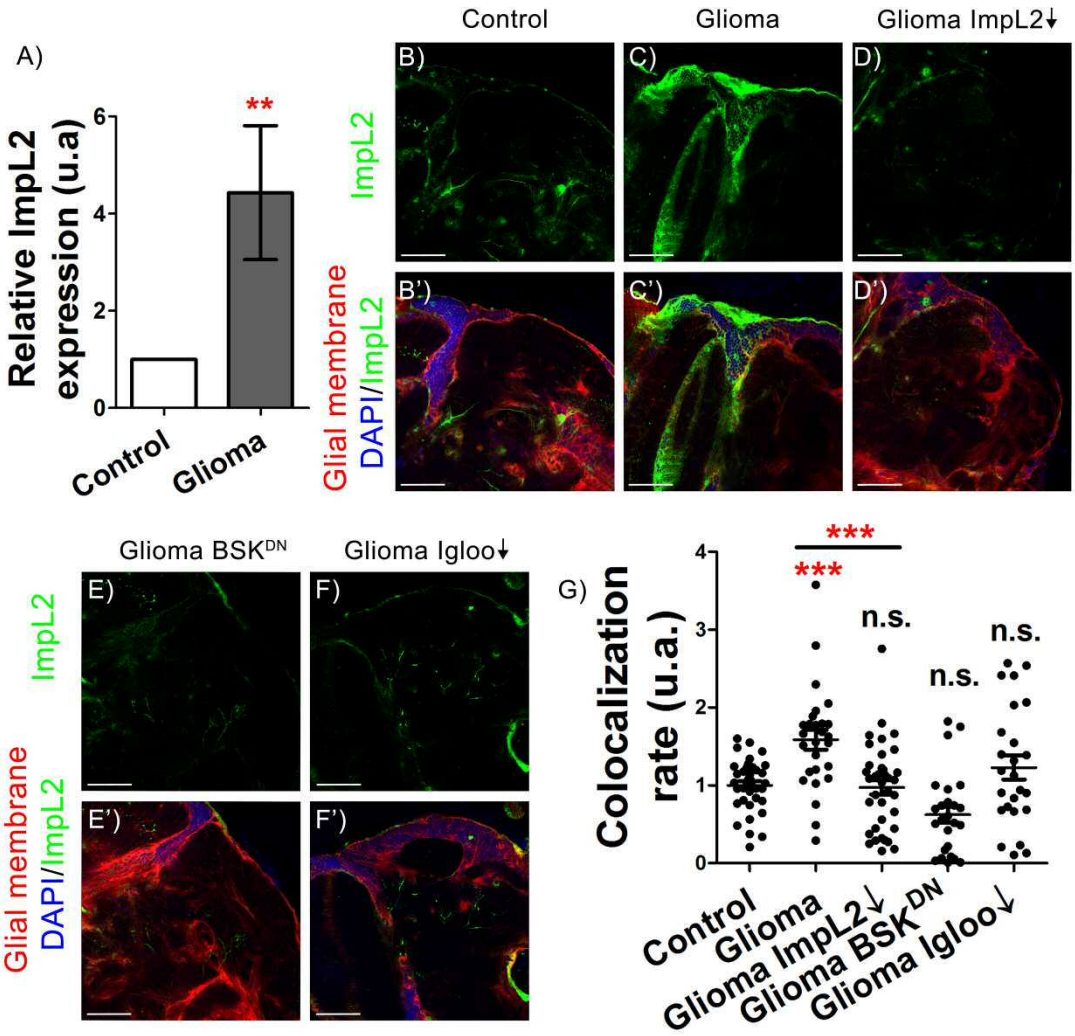

Fig 1. ImpL2 is upregulated in gliomas. A) RT-qPCR shows an upregulation of *ImpL2* in gliomas of repo> *UAS-dEGFR*$^{\lambda}$, *UAS-dp110*^{CAAX} flies (t-test). Confocal microscopy images of 7 day old adult brains from B) repo>LacZ (control), C) repo>UAS-dEGFR$^{\lambda}$, UAS-dp110CAAX (glioma), D) *repo>UAS-dEGFR*$^{\lambda}$*, UAS-dp110CAAX, Impl2 RNAi (*glioma>*ImpL2↓)*, E) *repo>UAS-dEGFR*$^{\lambda}$*, UAS-dp110CAAX, BSK*^{DN} (*glioma>BSK*^{DN}*)* and F) *repo>UAS-dEGFR*$^{\lambda}$*, UAS-dp110CAAX, igloo RNAi (glioma>igloo↓)* animals, in all cases together with an *ImpL2-MIMIC GFP* transgene. G) Quantification and statistical analysis of correlation rate between *Impl2-MIMIC GFP* and glial membrane in at least *N* = 10 per genotype (ANOVA, post-hoc Bonferroni).

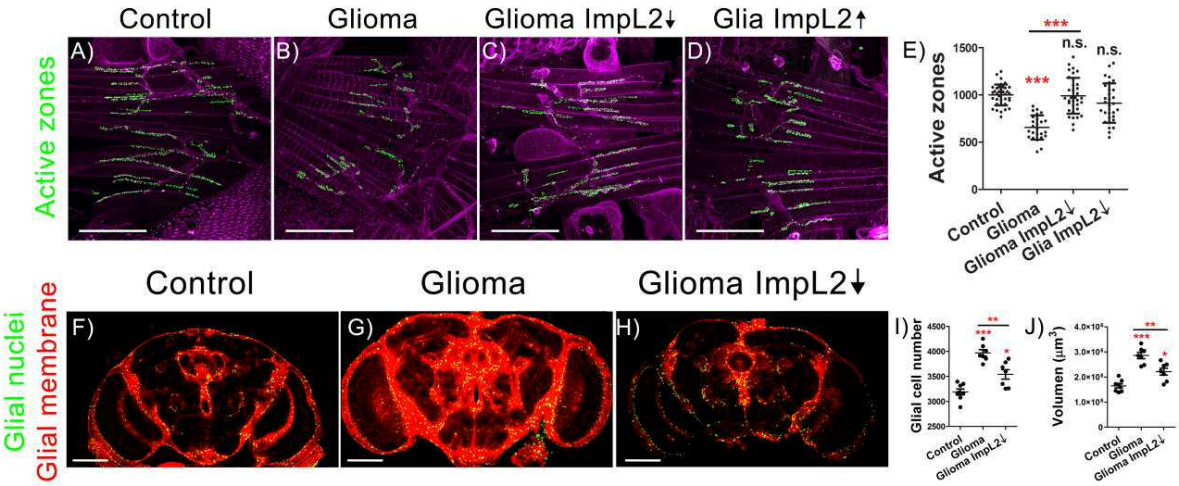

Fig 2. ImpL2 downregulation in glioma cells causes neurodegeneration and reduces tumor progression. Confocal Images of adult neuromuscular junction (NMJ) at 7th day at 29ºC from A) *repo>LacZ*, B) *repo>UAS-dEGFR$^{\lambda}$, UAS-dp110CAAX*, C) *repo>UAS-dEGFR$^{\lambda}$, UAS-dp110CAAX, Impl2 RNAi* and D) *repo>UAS-dEGFR$^{\lambda}$, UAS-dp110CAAX*, *ImpL2* animals. Active zones are marked in green (anti-NC82). E) Quantification and statistical analysis of active zones in at least *N* = 13 per genotype (ANOVA, post-hoc Bonferroni) (scale bar, 50 µm). Confocal microscopy images of adult brains from F) *repo>LacZ*, G) *repo>UAS-dEGFR$^{\lambda}$, UAS-dp110CAAX* and H) r*epo>UAS-dEGFR$^{\lambda}$, UAS-dp110CAAX, Impl2 RNAi* flies after 7 days at 29ºC. Glial membrane is in red and glial nuclei in green. Quantification of I) glial cell number and J) glial membrane volume for at least N = 7 per genotype (ANOVA, post-hoc Bonferroni) (scale bar, 100 µm). (**p*-value>0,05***p*-value>0,005, ****p*-value>0,0001)

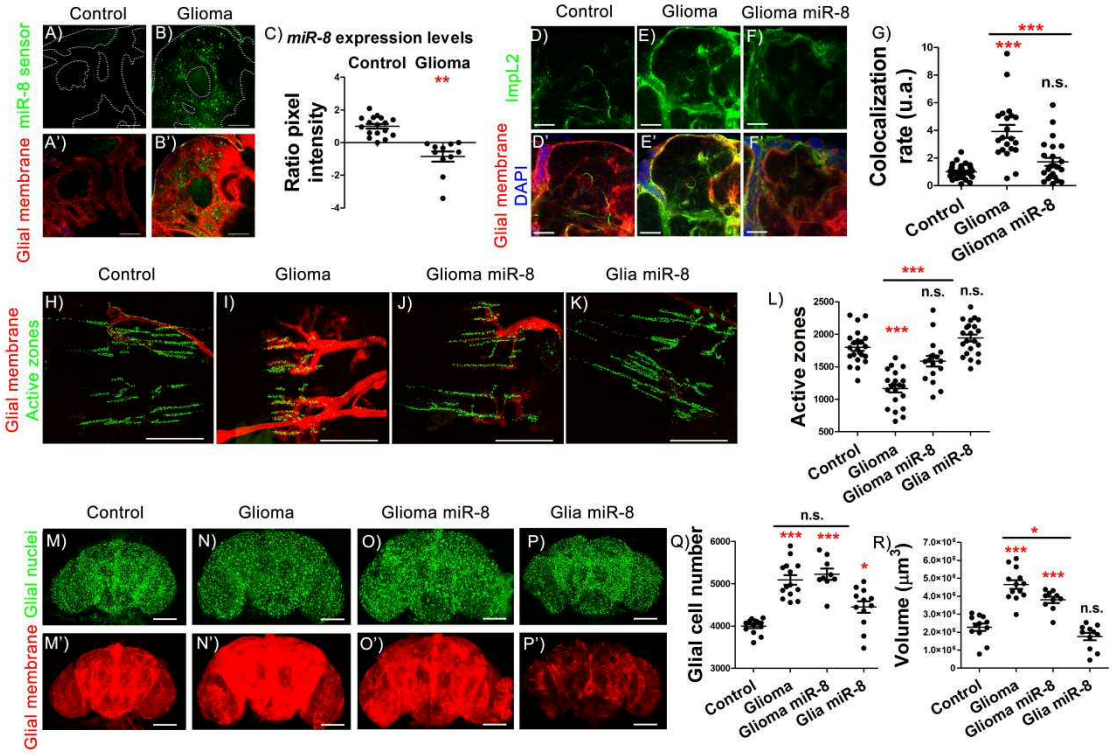

Fig 3. Increasing *miR-8* levels in gliomas impairs ImpL2 overexpression and synapse loss. A-B) Confocal microscopy images of adult brain showing the expression pattern of *miR-8* in *repo>LacZ* control animals compare to *repo>UAS-dEGFR$^{\lambda}$, UAS-dp110CAAX* flies using *miR-8* sensor (see Materials and Methods). A'-B') Glial membrane is marked in red. C) Quantification and statistical analysis of pixel intensity in at least *N* = 3 per genotype (ANOVA, post-hoc Bonferroni) (scale bar, 50 mm). Confocal microscopy images of adult brains from D) *repo>LacZ*, E) *repo>UAS-dEGFR$^{\lambda}$, UAS-dp110CAAX*, F) *repo>UAS-dEGFR$^{\lambda}$, UAS-dp110CAAX*, *miR-8* using an *ImpL2-MIMIC* line after 7 days at 29ºC. G) Quantification and statistical analysis of correlation rate in at least *N* = 9 per genotype (ANOVA, post-hoc Bonferroni). Adult neuromuscular junction (NMJ) from H) *repo>LacZ*, I) *repo>UAS-dEGFR$^{\lambda}$, UAS-dp110CAAX*, J) *repo>UAS-dEGFR$^{\lambda}$, UAS-dp110CAAX miR-8* and K) *repo>miR-8 after 7 days at 29ºC.* Active zones are marked in green. L) Quantification and statistical analysis of active zones number in at least *N* = 10 per genotype (ANOVA, post-hoc Bonferroni) (scale bar, 50 mm). Confocal microscopy images of adult brain from 7-day-old flies of M) *repo>LacZ*, N) *repo>UAS-dEGFR$^{\lambda}$, UAS-dp110CAAX*, O) *repo>UAS-dEGFR$^{\lambda}$, UAS-dp110CAAX miR-8* and P) *repo>LacZ, miR-8* genotypes. M'-P') Glial membrane is shown in red and glial nuclei in green. Quantification of Q) glial cells and R) glial membrane volume for at least N = 9 per genotype (ANOVA, post-hoc Bonferroni) (scale bar, 100 mm). (**p*-value>0,05***p*-value>0,005, ****p*-value>0,0001)

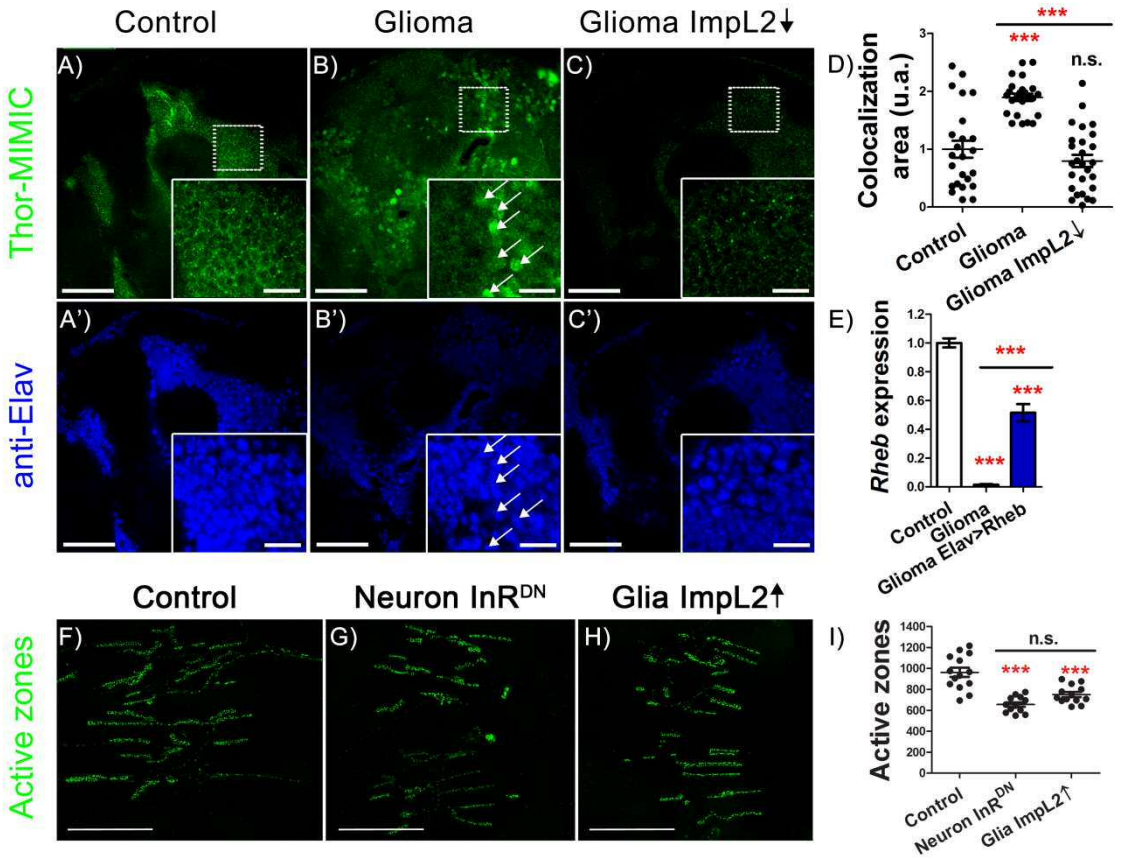

Fig 4. Glioma-secreted ImpL2 inhibits insulin pathway activity in neurons. Confocal microscopy images of adult brain of 7-day-old flies from A) *repo>LacZ*, B) *repo>UAS-dEGFR$^{\lambda}$, UAS-dp110CAAX* and C) *repo>UAS-dEGFR$^{\lambda}$, UAS-dp110CAAX*, *ImpL2 genotypes together with* a Thor-MIMIC transgene (showed in green). Neurons are marked in blue (A'-C'). D) Quantification and statistical analysis of correlation area in *N* = 9 per genotype (ANOVA, post-hoc Bonferroni) (scale bar, 50 μm/10 μm).) RT-qPCR of *Rheb* expression is downregulated in gliomas and the ectopical expression in neurons rescues the phenotype (ANOVA, post-hoc Bonferroni). Adult neuromuscular junction (NMJ) from F) *D42>LacZ*, G) *D42>InR^{DN}* and H) *repo>ImpL2* animals after 7 days at 29ºC (active zones shown in green). *D42* is expressed in motor neurons. I) Quantification and statistical analysis of active zones in at least *N* = 20 per genotype (ANOVA, post-hoc Bonferroni) (scale bar, 50 μm) (***p-value>0,0001).

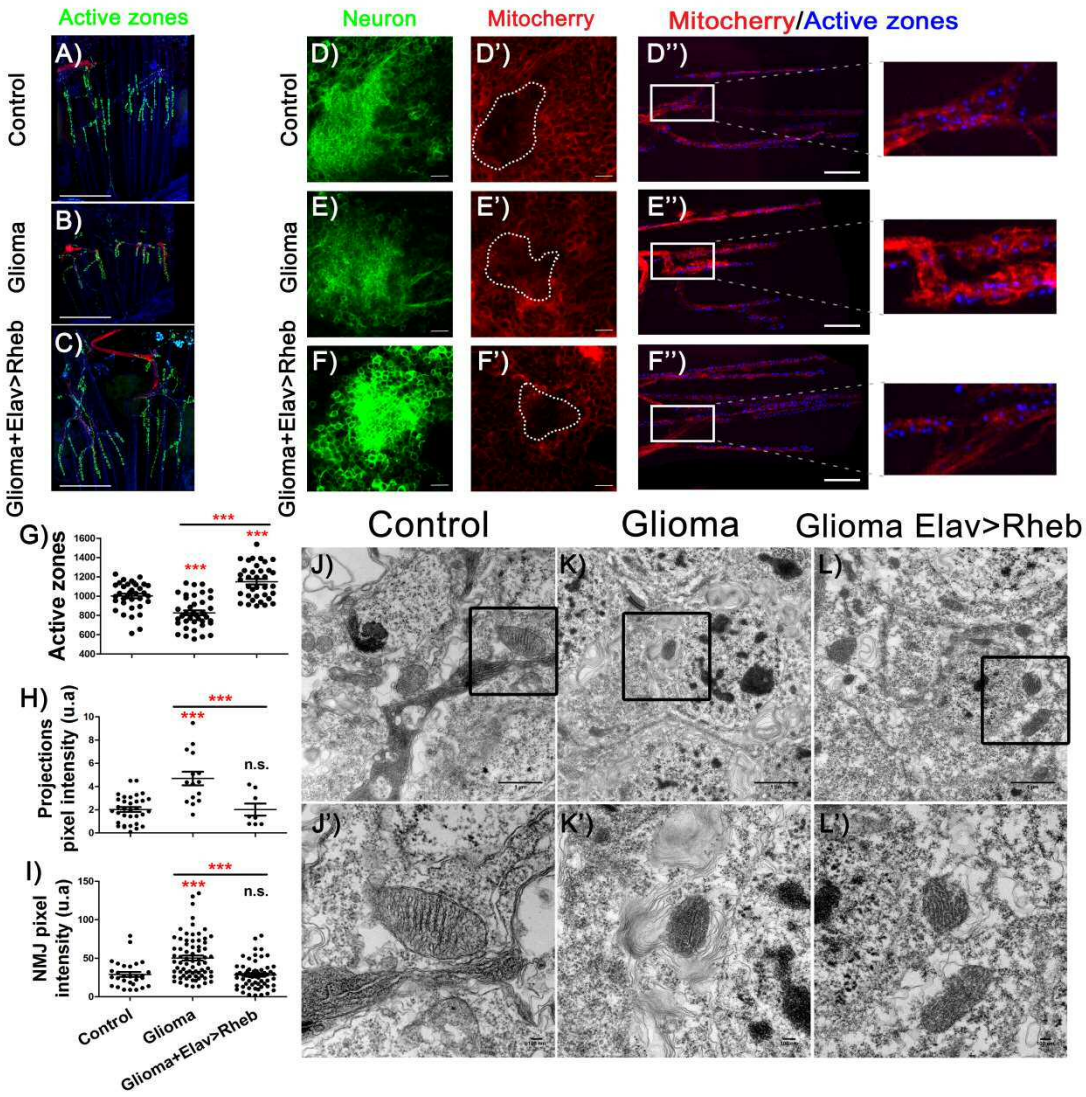

Fig 5. Glioma-induced mitochondrial alterations are rescue by *Rheb* expression. Adult neuromuscular junction (NMJ) from A) repo>LacZ, B) repo>UAS-dEGFR$^{\lambda}$, UAS-dp110CAAX and C) repo>UAS-dEGFR$^{\lambda}$, UAS-dp110CAAX; *elav-LexA, LexAOp-Rheb* after 7 days at 29ºC (active zones are marked in green). G) Quantification and statistical analysis of active zones number in at least *N* = 20 per genotype (ANOVA, post-hoc Bonferroni) (scale bar, 50 μm). Confocal microscopy images of adult brain and NMJ from D) control, E) repo>LacZ and F) repo>UAS-dEGFR$^{\lambda}$, UAS-dp110CAAX; *elav-LexA, LexAOp-Rheb* after 7 days at 29ºC (neural membrane shown in green), D'-F') mitochondrial membrane in red and D''-F'') active zones in blue (scale bar,). Quantification and statistical analysis of pixel intensity in H) projections and I) NMJ in at least *N* = 15 and *N* = 3 respectively per genotype (ANOVA, post-hoc Bonferroni). Electron microscopy images of neurons from brains of adult flies of J) *repo>LacZ*, K) *repo>UAS-dEGFR$^{\lambda}$, UAS-dp110CAAX* and L) *repo>UAS-dEGFR$^{\lambda}$, UAS-dp110CAAX; elav-LexA, LexAOp-Rheb* and an amplification from black square of mitochondria in detail (J'-L') (scale bar, 1 mm/ 100 nm respectively).

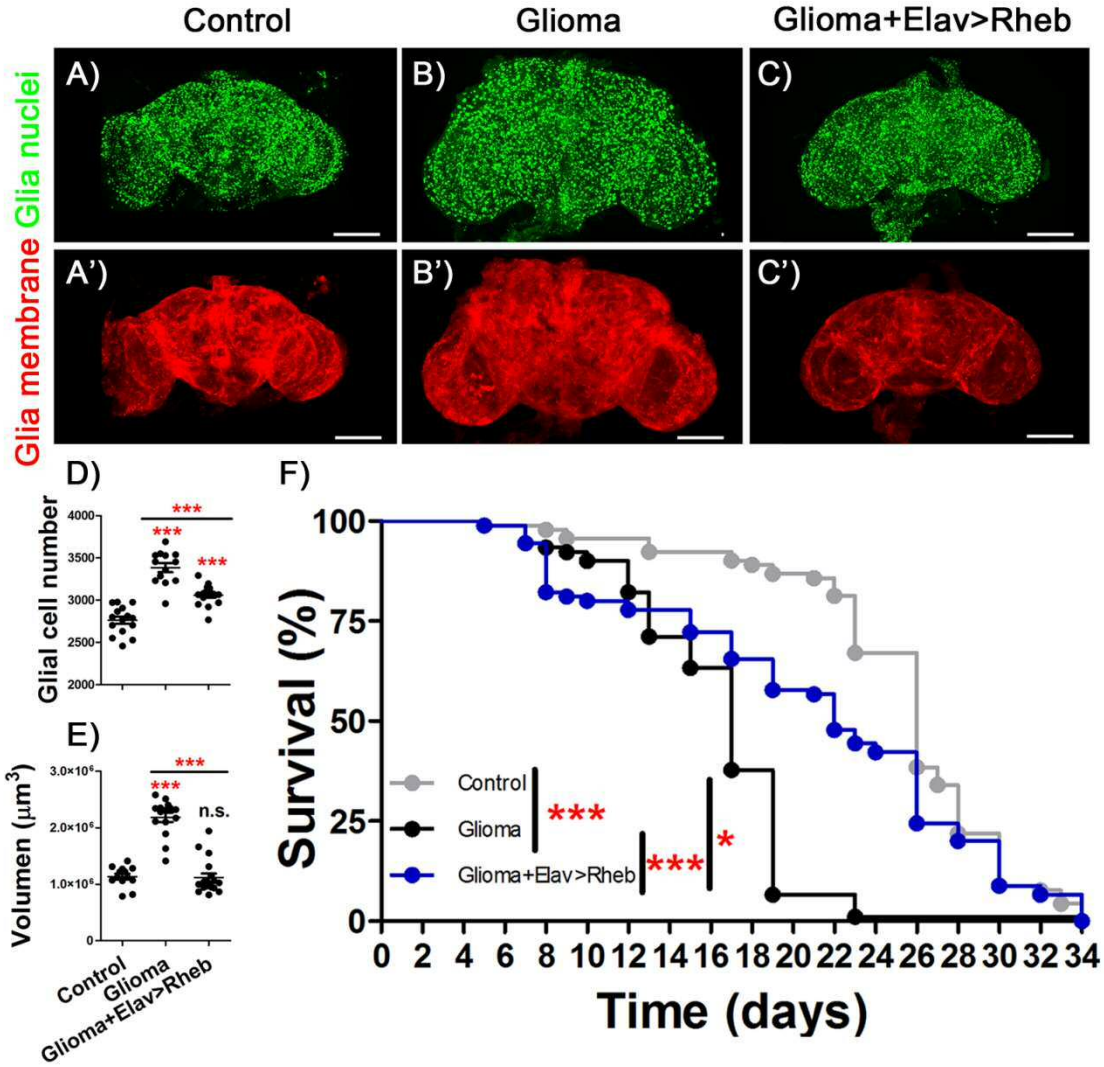

Fig 6. Overexpression of *Rheb* in neurons seems to be protective against glioma effects. Confocal microscopy images of adult brains from A) *repo>LacZ*, B) *repo>UAS-dEGFR$^{\lambda}$, UAS-dp110CAAX* and C) *repo>UAS-dEGFR$^{\lambda}$, UAS-dp110CAAX; elav-LexA, LexAOp-Rheb* after 7 days at 29ºC with glial nuclei marked in green. A'-C') Glial membrane is shown in red. D) Glial cells number quantification and E) glial membrane volume quantification for at least N = 13 per genotype (ANOVA, post-hoc Bonferroni) (scale bar, 100 μm). F) Graph shows a survival assay of *repo>LacZ* (grey), *repo>UAS-dEGFR$^{\lambda}$, UAS-dp110CAAX* (black) and *repo>UAS-dEGFR$^{\lambda}$, UAS-dp110CAAX, elav-LexA, LexAOp-Rheb* (blue) flies and statistical analysis in *N* = 90 (Mantel-Cox test) (**p*-value>0,05,***p*-value>0,005, ****p*-value>0,0001).